Neutron activation of Ga-69 and Ga-71 at k(B)T approximate to 25 keV

Neutron activation of ^{69}Ga and ^{71}Ga at $k_BT \approx 25$ keV

Kathrin Göbel,[1,*] Clemens Beinrucker,[1] Benjamin Brückner,[1] Philipp Erbacher,[1] Stefan Fiebiger,[1] Micaela Fonseca,[2,3] Michael Heftrich,[1] Tanja Heftrich,[1] Franz Käppeler,[4] Antonin Krása,[5,6] Deniz Kurtulgil,[1] Claudia Lederer-Woods,[1,7] Ralf Plag,[1,8] Arjan Plompen,[5] René Reifarth,[1] Stefan Schmidt,[1] Kerstin Sonnabend,[1] and Mario Weigand[1]

[1]*Goethe-Universität Frankfurt am Main, Germany*
[2]*LIBPhys-UNL, DF, FCT, Universidade Nova de Lisboa, 2829-516 Caparica, Portugal*
[3]*Digital Human-environment Interaction Labs, Universidade Lusófona de Humanidades e Tecnologia, Lisbon, Portugal*
[4]*Karlsruhe Institute of Technology, Germany*
[5]*European Commission, Joint Research Centre, Geel, Belgium*
[6]*SCK CEN, Mol, Belgium*
[7]*University of Edinburgh, United Kingdom*
[8]*GSI Helmholtzzentrum für Schwerionenforschung, Darmstadt, Germany*

(Received 8 September 2020; accepted 19 January 2021; published 12 February 2021)

Background: About 50% of heavy elements are produced by the slow neutron capture process (*s* process) in stars. The element gallium is mostly produced during the weak *s* process in massive stars.
Purpose: Our activation at $k_BT \approx 25$ keV is the first experiment in a series of activation and time-of-flight measurements on ^{69}Ga and ^{71}Ga relevant for astrophysics.
Methods: We activated ^{69}Ga and ^{71}Ga with a neutron distribution that corresponds to a quasistellar distribution with $k_BT = 25$ keV at the Joint Research Centre (JRC), Geel, Belgium. Protons were provided by an electrostatic Van de Graaff accelerator to produce neutrons via the reaction ^{7}Li(p, n). The produced activity was measured via the γ emission by the decaying product nuclei by high-purity germanium detectors.
Results: We provide spectrum-averaged cross sections (SACS) and ratios of the cross sections σ_{Ga}/σ_{Au} for the neutron spectrum of the activation. We obtain values of $\sigma_{69Ga,SACS} = (186 \pm 12)$ mb and $\sigma_{71Ga,SACS} = (112 \pm 7)$ mb, and cross-section ratios of $\sigma_{69Ga}/\sigma_{Au} = 0.29 \pm 0.02$ and $\sigma_{71Ga}/\sigma_{Au} = 0.17 \pm 0.01$.
Conclusions: Our data disagree with the available evaluated data provided by KADoNiS v0.3, our cross-section ratio is about 20% higher for ^{69}Ga and about 20% lower for ^{71}Ga.

DOI: 10.1103/PhysRevC.103.025802

I. INTRODUCTION

Most of the elements heavier than iron are produced by the slow (*s*) and the rapid (*r*) neutron capture processes. The *s* process takes place during stellar helium and carbon burning phases with neutron densities between 10^6 and 10^{12} cm^{-3} [1]. The *s* process is composed of the weak and the main component [2]. The components mainly differ in the neutron-to-seed ratios, the temperatures and the neutron densities. The main component of the *s* process takes place at about $k_BT = 5$ to 25 keV in low-mass asymptotic giant branch (AGB) stars and contributes mostly to the nuclei with mass numbers above $A = 90$. The weak *s* process at 25 and 90 keV in massive stars with more than eight solar masses produces most of the *s*-process isotopes between iron and strontium ($60 < A < 90$). The main neutron source is provided by the reaction ^{22}Ne$(\alpha, n)^{25}$Mg at the end of the convective He-burning-core and in the following convective C-burning-shell phases [1,3,4]. The neutron fluence in the weak *s* process is too low to achieve reaction flow equilibrium, in contrast to the main *s*-process component. Therefore, a particular neutron capture cross section not only determines the abundance of the respective isotope (as in the case of the main component), but affects the abundances of all heavier isotopes as well [5,6]. The element gallium is mostly produced during the weak *s* process in massive stars (see Fig. 1). Simulations [4] show that gallium is the most abundant *s* element at the end of shell carbon burning.

Our activation at $k_BT \approx 25$ keV is the first experiment in a series of activation and time-of-flight measurements on ^{69}Ga and ^{71}Ga relevant for astrophysics.

Available experimental data in the keV regime

Data from two activation measurements are available for ^{69}Ga. Both experiments used Sb-Be sources, which produce nearly monoenergetic neutrons with a dominant peak at 23 keV (97%) and an additional peak at 378 keV (3%). The obtained neutron capture cross sections, (148.4 ± 1.2) mb [7,8] and (50 ± 5) mb [8,9], disagree by a factor of three.

Also for ^{71}Ga, two activation experiments with Sb-Be sources were carried out. The resulting cross sections are

*goebel@physik.uni-frankfurt.de

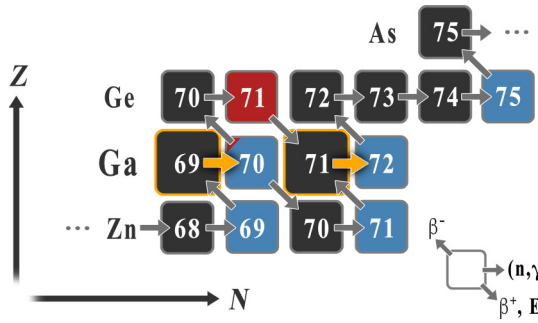

FIG. 1. Path of the *s* process between zinc and arsenic. When ^{69}Ga captures a neutron, the product ^{70}Ga either decays to ^{70}Ge or ^{70}Zn with a half-life of 21.14 minutes. Following the neutron capture reaction on ^{71}Ga, the product ^{72}Ga decays to ^{72}Ge with a half-life of 14.1 hours. The neutron capture reactions on ^{69}Ga and ^{71}Ga are marked in yellow.

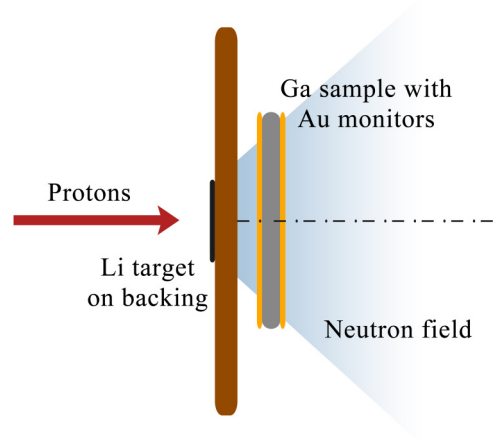

FIG. 2. Sketch of the activation setup. A proton beam impinges on a lithium target. The neutron cone covers an angle of 120° for the 1912 keV proton beam. The gallium samples were mounted with one gold monitor on each side.

(140 ± 30) mb [8,10] and (75 ± 10) mb [8,9]. A measurement with a monoenergetic filtered neutron beam with $E_n = (25 \pm 5)$ keV yields a value of (104 ± 14) mb [8,11]. References [12,13] obtain a value of 138 mb for an integral measurement with a neutron distribution that corresponds to a quasistellar distribution with $k_BT = 25$ keV.

In addition, Dovbenko *et al.* carried out activation measurements for ^{69}Ga and ^{71}Ga in the energy range from 10 to 350 keV with quasimonoenergetic neutrons [8,14]. At (27 ± 5.3) keV, neutron capture cross sections of (172 ± 49) mb for ^{69}Ga and (159 ± 45) mb for ^{71}Ga were obtained.

So far, time-of-flight measurement data are only available for natural gallium [15]. However, other nuclei (^{81}Br, ^{75}As, ^{74}Ge) measured within the same experimental campaign show large deviations from more recent results [13].

To improve the experimental-data availability, we carried out an activation experiment with a neutron distribution that corresponds to a quasistellar distribution with $k_BT = 25$ keV.

II. THE ACTIVATION EXPERIMENT

The activation was carried out at the European Commission Joint Research Centre (EC-JRC), Geel, Belgium. An electrostatic 7 MV Van de Graaff accelerator accelerated protons to produce neutrons via the reaction ^{7}Li(p, n). The proton energy was 1912 keV to produce a neutron distribution that corresponds to a quasistellar distribution with $k_BT = 25$ keV [16]. The neutron production targets were water cooled during the activation to dissipate heat load. The neutron flux was monitored by a BF_4 ionization chamber. Samples of natural gallium were positioned between two gold monitors (see Fig. 2). The beam parameters and the properties of the lithium and the gallium samples are given in Table I.

A. Sample characteristics

We used two samples of natural gallium for the activation experiment, Ga I with a mass of 460.95 mg ± 0.02% and Ga II with a mass of 604.50 mg ± 0.02%. Natural gallium consists of 60.11% ^{69}Ga and 39.89% ^{71}Ga [17]. The samples were positioned between two gold monitors, Au Ia (61.10 mg) and Au Ib (65.16 mg) during the activation with Ga I, and Au IIa (108.9 mg) and Au IIb (109.1 mg) together with Ga II. The number of nuclei calculated from the sample masses and the half-lives are summarized in Table II. We neglect the uncertainties in the numbers of nuclei in the following.

B. Neutron spectrum

The resulting neutron spectrum for the gallium sample was simulated with the program PINO (Proton In Neutron Out) [21] and is shown in Fig. 3. The Monte Carlo simulation includes the geometry of the Li layer, the energy loss in the lithium layer, the geometry and position of the sample and the spread of the proton energy (see Table I). The resulting distribution is in good agreement with the stellar Maxwell-Boltzmann distribution for $k_BT = 25$ keV except for the high-energy tail [22,23].

III. ANALYSIS

We determined the ratio of the cross sections of neutron captures on gallium and gold by

$$\frac{\sigma_{\mathrm{Ga}}}{\sigma_{\mathrm{Au}}} = \frac{\frac{P_{\mathrm{Ga}}}{N_{\mathrm{Ga}}}}{\frac{1}{2}\left(\frac{P_{\mathrm{Au\,a}}}{N_{\mathrm{Au\,a}}} + \frac{P_{\mathrm{Au\,b}}}{N_{\mathrm{Au\,b}}}\right)}. \quad (1)$$

TABLE I. Beam parameters, properties of the lithium and gallium samples, and geometry of the activation setup.

Proton energy	1912 ± 2 keV
Lithium target	
Thickness	27.5 μm
Radius	3 mm
Ga activation sample	
Distance to lithium	1 mm
Radius	6 mm

TABLE II. Characteristics of the gallium and gold samples.

Sample		$N_{\text{sample}}/10^{20}$	$t_{1/2}$ of product
Ga I	^{69}Ga	$23.931 \pm 0.02\%$	21.14 (5) min [18]
	^{71}Ga	$15.882 \pm 0.02\%$	14.10 (2) h [19]
Au Ia	^{197}Au	$1.868 \pm 0.02\%$	2.6941 (2) d [20]
Au Ib	^{197}Au	$1.992 \pm 0.02\%$	
Ga II	^{69}Ga	$31.384 \pm 0.02\%$	
	^{71}Ga	$20.828 \pm 0.02\%$	
Au IIa	^{197}Au	$3.330 \pm 0.10\%$	
Au IIb	^{197}Au	$3.336 \pm 0.10\%$	

The numbers of sample nuclei N were determined by the sample masses. The numbers of produced nuclei, P, were calculated from the counts C in the respective γ line with several correction factors:

$$P = \frac{C}{f_b f_{wm} f_d f_{sim}}. \quad (2)$$

The factor f_b corrects for the decays during the activation, f_{wm} corrects for the decays before and after the measurement, and f_d corrects for the dead time of the data acquisition system. The factor f_{sim} accounts for the γ intensity I_γ, the detector efficiency ϵ, the self-absorption κ, and the coincidence summing and was determined in GEANT3 simulations of the counting geometry, see Sec. III B.

A. γ-ray spectrometry

The number of activated nuclei was determined by γ-ray spectrometry with high-purity germanium detectors. In the case of ^{69}Ga we used the γ lines with energies of 176 keV and 1039 keV from the decay of ^{70}Ga, in the case of ^{71}Ga we used the γ lines at 601, 629, 834, 894, and 1051 keV from the decay of ^{72}Ga. Higher-energy γ lines were not considered because the efficiency was only determined up to about 1330 keV using calibration sources. The values obtained are given in Table III. Figure 4 shows the spectrum of the Ga II sample after activation. We used the 411.8 keV line from the decay of ^{198}Au to determine the number of activated gold nuclei. The results are given in Table IV.

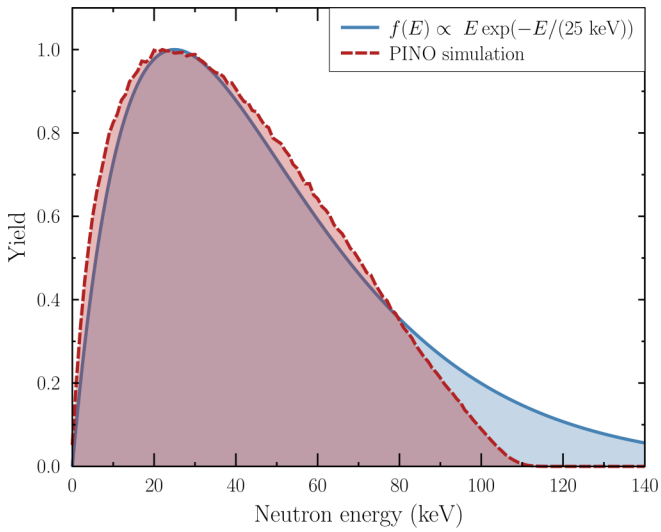

FIG. 3. Simulated neutron spectra (red) with a peak energy at 25 keV [21]. The parameters for the simulation are given in Table I. The Maxwell-Boltzmann distribution for $k_BT = 25$ keV is shown in blue.

B. Simulations of the counting geometry

We simulated the counting geometry using GEANT3 to obtain the correction factors for the self-absorption of the γ rays in the sample and the coincidence summing correction. The detector geometry with its germanium crystal, detector window, cooling finger, and accumulated dead layer was varied to reproduce the efficiency as a function of the γ-line energy that had been obtained by a fit to measurements with calibration sources. The list of calibration sources is given in Table V. The simulations were carried out for the energies of the γ lines of the calibration sources, the γ lines from the decays of ^{70}Ga and ^{72}Ga used in our analysis and for 10, 20, 50, 100, 200, 500, and 1000 keV.

Figure 5 shows the fit to the measurements with calibration sources and its uncertainty band of 3.9%. The values obtained from the GEANT3 simulations agree with the fit within its uncertainty.

C. Time corrections

The decays of freshly produced nuclei during the irradiation have to be taken into account with the correction factor f_b. The fluctuation of the neutron flux was monitored in intervals of three minutes with a BF_4 filled ionization chamber via the ^{10}B(n, α) ^{7}Li reaction. The correction factors for the gallium and gold samples were calculated via

$$f_b = \frac{\sum_i \Phi_i \exp\left[-\lambda(t_a - i\Delta t)\right]}{\sum_i \Phi_i}, \quad (3)$$

with the neutron-detector counts Φ_i for each time interval Δt, the duration of the activation t_a and the decay constant λ of the activation product. The uncertainties of the factors f_b are less than 0.1% and are neglected in the following.

The decays before and after the measurement are corrected for by the factor f_{wm}:

$$f_{wm} = \exp(-\lambda t_w)[1 - \exp(-\lambda t_m)], \quad (4)$$

where λ is the decay constant, t_w is the time between the activation and the measurement, and t_m is the duration of the measurement.

To determine the dead time, a series of calibration source measurements with varying distance to the HPGe detector and, hence, varying count rate, was carried out. The fraction of dead time could be described by a second-degree polynomial function:

$$F_d = (-3.531 \times 10^{-8})c^2 + (5.673 \times 10^{-5})c + 8.297 \times 10^{-4}, \quad (5)$$

where F_d is the fraction of dead time and c is the number of counts per second. The correction factor f_d is calculated by

$$f_d = 1 - F_d. \quad (6)$$

TABLE III. The number of counts determined during counting at the HPGe detector for the γ lines of the gallium samples, corresponding γ intensities of ^{70}Ga [18] and ^{72}Ga [19], and the correction factor $f_{\rm sim}$ calculated from the results of the Monte Carlo simulations.

		Counts			$f_{\rm sim}$	
Decay of	γ energy (keV)	Ga I	Ga II	I_γ (%)	Ga I	Ga II
^{70}Ga	176.115 (13)	7258 (104)	9908 (121)	0.294 (9)	0.000374 ± 6%	0.000375 ± 6%
	1039.513 (10)	7976 (93)	11068 (108)	0.65 (5)	0.000358 ± 9%	0.000359 ± 9%
^{72}Ga	600.912 (15)	1783 (59)	2085 (65)	5.822 (19)	0.00276 ± 5%	0.00268 ± 5%
	629.967 (19)	9493 (105)	11265 (115)	26.13 (4)	0.0133 ± 5%	0.0134 ± 5%
	834.13 (4)	34455 (188)	40371 (204)	95.45 (8)	0.0491 ± 5%	0.0489 ± 5%
	894.327 (18)	2672 (58)	3232 (62)	10.136 (15)	0.00388 ± 5%	0.00378 ± 5%
	1050.794 (17)	1668 (46)	1853 (49)	6.991 (11)	0.00244 ± 5%	0.00243 ± 5%

The uncertainty in the dead-time correction of 0.6% results from the uncertainties of the γ-line intensities.

The time correction factors for the gallium and gold samples are summarized in Table VI. The corrections for the decays during the activation ($f_{\rm b}$) for ^{72}Ga and ^{198}Au are close to 1 because of their long half-lives compared with the activation time of 40 minutes, while $f_{\rm b}$ is almost 50% for ^{70}Ga with its half-life of about 21 minutes. Similarly, the correction factors for the decays before and after the measurement are much smaller for ^{70}Ga than for ^{72}Ga and ^{198}Au. The dead-time correction is small in all cases as the count rates were in the order of only a few hundred counts per second.

D. Number of freshly produced nuclei

We calculate the number of freshly produced nuclei with the number of counts determined during counting at the HPGe detector for the investigated γ lines of the gallium and gold samples, taking into account all correction factors. The results are shown in TableVII. We determined the systematic uncertainties by the uncertainties of the simulation and of the γ-line intensities. Hence, the contributions from the correction factors $f_{\rm b}$, $f_{\rm wm}$, and $f_{\rm d}$ will be neglected in the following analysis.

E. Results

We determined the ratio of the cross sections $\sigma_{\rm Ga}/\sigma_{\rm Au}$ for the neutron capture reactions on ^{69}Ga and ^{71}Ga for all γ lines mentioned in Sec. III A and for the neutron spectrum shown in Fig. 3. The results are shown in Table VIII. The statistical and systematic uncertainties are calculated by error propagation of the values in Table VII.

We calculated the weighted mean for each reaction with

$$\bar{x} = \sum_{i=1}^{n} \frac{x_i}{u_{\rm tot}^2} \Bigg/ \sum_{i=1}^{n} \frac{1}{u_{\rm tot}^2}, \tag{7}$$

where $u_{\rm tot}$ is the total uncertainty, namely, the quadratic sum of $u_{\rm stat}$ and $u_{\rm syst}$:

$$u_{\rm tot}^2 = u_{\rm stat}^2 + u_{\rm syst}^2. \tag{8}$$

The uncorrelated uncertainties of the weighted mean cross-section ratio include the statistical uncertainties of the counts determined by γ-ray spectrometry and the uncertainties of the γ-line intensities I_γ. We determined their weighted mean using

$$\bar{u}_{\rm uncorr} = \left[\sum_{i=1}^{n} \frac{1}{u_{i,\rm uncorr}^2} \right]^{-1/2}. \tag{9}$$

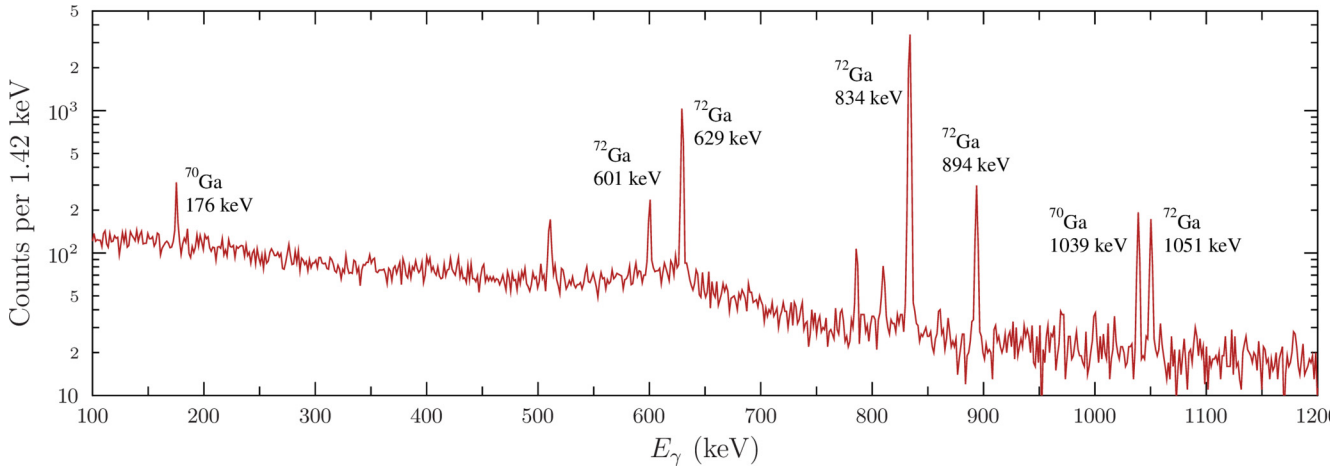

FIG. 4. Result of the γ counting after the activation of the sample Ga II. We used the two γ lines from the decay of ^{70}Ga and the five γ lines with the highest γ intensities from the decay of ^{72}Ga for the analysis.

TABLE IV. The number of counts for the 411.8 keV γ line determined during counting at the HPGe detector for the gold samples. The corresponding γ intensity is $95.62 \pm 0.02\%$ [20]. The correction factor f_{sim} was calculated from the results of the Monte Carlo simulations.

Sample	Counts	f_{sim}
Au Ia	10631 (116)	$0.102 \pm 5\%$
Au Ib	10591 (111)	$0.102 \pm 5\%$
Au IIa	45049 (238)	$0.101 \pm 5\%$
Au IIb	44915 (240)	$0.101 \pm 5\%$

The correlated uncertainties include the systematic uncertainties in Table VIII. We give the mean correlated uncertainties.

The weighted mean of the cross-section ratio $\sigma_{\text{Ga}}/\sigma_{\text{Au}}$ for the reaction ^{69}Ga(n, γ) is

$$\left\langle \frac{\sigma_{69\text{Ga}}}{\sigma_{197\text{Au}}} \right\rangle = 0.2862 \pm 0.0062_{\text{uncorr}} \pm 0.0182_{\text{corr}},$$

and for ^{71}Ga(n, γ)

$$\left\langle \frac{\sigma_{71\text{Ga}}}{\sigma_{197\text{Au}}} \right\rangle = 0.1727 \pm 0.0007_{\text{uncorr}} \pm 0.0107_{\text{corr}}.$$

To determine the neutron capture cross sections of ^{69}Ga and ^{71}Ga we folded the evaluated ^{197}Au neutron capture cross section [16] with the neutron spectrum in our activation experiment [21]. We obtained a value for the spectrum-averaged neutron capture cross section of $\sigma_{197\text{Au,SACS}} = (650 \pm 6)$ mb. We calculate the SACSs to

$$\sigma_{69\text{Ga,SACS}} = (186 \pm 12) \text{ mb},$$
$$\sigma_{71\text{Ga,SACS}} = (112 \pm 7) \text{ mb}.$$

IV. DISCUSSION

A. Comparison with KADoNiS v0.3

In a first step, we compare our results to evaluated data provided by KADoNiS v0.3 [13]. The database recommends the Maxwellian-averaged cross sections $\sigma_{69\text{Ga,MACS}} = 153$ mb for ^{69}Ga and $\sigma_{71\text{Ga,MACS}} = 138$ mb for ^{71}Ga for $k_BT = 25$ keV, only taking into account the data by Walter *et al.* [15]. Here, as in our results, the SACS for ^{69}Ga is higher than that of ^{71}Ga.

The neutron spectrum in our experiment is very similar to a spectrum corresponding to $k_BT = 25$ keV. For a sound comparison, we compare the cross-section ratios between ^{69,71}Ga and ^{197}Au for SACS and MACS since they are largely independent of small spectrum deviations. For 25 keV we calculate the MACS cross-section ratios from KADoNiS v0.3:

$$\text{KADoNiS: } \sigma_{69\text{Ga,MACS}}/\sigma_{197\text{Au,MACS}} = 0.24 \pm 0.01,$$
$$\text{KADoNiS: } \sigma_{71\text{Ga,MACS}}/\sigma_{197\text{Au,MACS}} = 0.21 \pm 0.01.$$

Within the uncertainties given in the database the ratios are valid from $k_BT = 15$ keV to $k_BT = 50$ keV and, hence, can be compared with our results.

Our data disagree with the evaluated data, our cross-section ratio is about 20% higher for ^{69}Ga and about 20% lower for ^{71}Ga.

TABLE V. Calibration sources and the γ lines used to determine the detector efficiency.

Isotope	γ energy (keV)
^{241}Am	59.5
^{109}Cd	88.0
^{57}Co	122.1
^{57}Co	136.5
^{139}Ce	165.9
^{51}Cr	320.1
^{113m}In (product of ^{113}Sn)	391.7
^{85}Sr	514.0
^{137m}Ba (product of ^{137}Cs)	661.7
^{54}Mn	834.8
^{65}Zn	1115.5
^{60}Co	1173.2
^{60}Co	1332.5

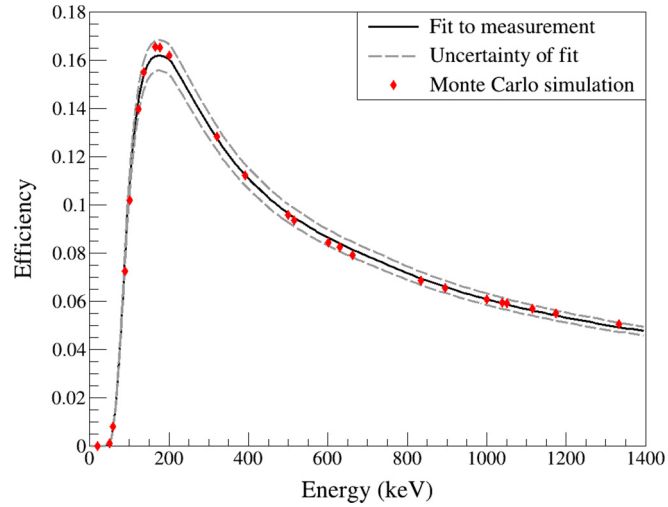

FIG. 5. γ efficiency of the HPGe detector as a function of γ energy. The black solid line is the fit to measurements with the calibration sources. The gray dashed lines show the uncertainty band of 3.9%. The red markers display the efficiencies obtained in the Monte Carlo simulations with an optimized detector geometry. They agree with the fit within its uncertainty.

TABLE VI. Corrections for the decays during the activation (f_{b}), before and after the measurement (f_{wm}), as well as for the dead time of the data acquisition (f_{d}).

Sample		f_{b}	f_{wm}	f_{d}
Ga I	^{70}Ga	0.540	$0.6917 \pm 0.2\%$	$0.988 \pm 0.6\%$
	^{72}Ga	0.983	$0.0322 \pm 0.2\%$	$0.988 \pm 0.6\%$
Ga II	^{70}Ga	0.540	$0.4629 \pm 0.3\%$	$0.981 \pm 0.6\%$
	^{72}Ga	0.983	$0.0181 \pm 0.3\%$	$0.981 \pm 0.6\%$
Au Ia		0.996	$0.00712 \pm 0.1\%$	$0.988 \pm 0.6\%$
Au Ib		0.996	$0.00663 \pm 0.1\%$	$0.998 \pm 0.6\%$
Au IIa		0.996	$0.01012 \pm 0.2\%$	$0.999 \pm 0.6\%$
Au IIb		0.996	$0.01054 \pm 0.2\%$	$0.999 \pm 0.6\%$

TABLE VII. Number of freshly produced nuclei P for all samples in both activations. The statistical uncertainties u_{stat} result from the uncertainties of the counts from the γ-ray spectrometry, the systematic uncertainties u_{syst} include the uncertainties of the γ intensities and of the correction factors f_{sim}.

Sample	Isotope	γ energy (keV)	$P/10^7$	u_{stat} (%)	u_{syst} (%)
Ga I	^{70}Ga	176	5.25	1.4	6.0
		1039	6.03	1.2	9.0
	^{72}Ga	601	2.06	3.3	5.0
		630	2.28	1.1	5.0
		834	2.24	0.6	5.0
		894	2.20	2.2	5.0
		1051	2.19	2.8	5.0
Au Ia	^{198}Au	411	1.49	1.1	5.0
Au Ib	^{198}Au	411	1.58	1.1	5.0
Ga II	^{70}Ga	176	10.8	1.2	6.0
		1039	12.6	1.0	9.0
	^{72}Ga	601	4.46	3.1	5.0
		630	4.82	1.0	5.0
		834	4.73	0.5	5.0
		894	4.90	1.9	5.0
		1051	4.37	2.6	5.0
Au IIa	^{198}Au	411	4.43	0.5	5.0
Au IIb	^{198}Au	411	4.24	0.5	5.0

B. Comparison with ENDF/B-VIII.0

As a second step, we compare our results to evaluated data provided by ENDF/B-VII.1 [24], which take into account the available experimental data mentioned in Sec. I as well as thermal and higher-energy neutron capture cross-section data. From Ref. [25] we obtain the data for 25 keV:

$$\text{ENDF: } \sigma_{69\text{Ga,MACS}} = 132 \text{ mb},$$

$$\text{ENDF: } \sigma_{71\text{Ga,MACS}} = 137 \text{ mb}.$$

We calculate the ratios of the cross sections from the MACSs with $\sigma_{197\text{Au,MACS}} = 682$ mb [25]:

$$\text{ENDF: } \sigma_{69\text{Ga,SACS}}/\sigma_{197\text{Au,SACS}} = 0.194,$$

$$\text{ENDF: } \sigma_{71\text{Ga,SACS}}/\sigma_{197\text{Au,SACS}} = 0.201.$$

Our data significantly disagree with the evaluated data; in particular, we obtain a cross-section ratio σ_{Ga}/σ_{Au} and accordingly a SACS for ^{69}Ga that is higher than that of ^{71}Ga, as expected from the decreasing binding energy with increasing neutron number. However, we want to point out that ENDF provides only insufficient data points for the reaction ^{71}Ga(n, γ) in the keV region, which introduces large uncertainties when calculating the MACS.

TABLE VIII. Ratios of the gallium and gold cross sections and its statistical and systematic uncertainties for the reactions ^{69}Ga(n, γ) and ^{71}Ga(n, γ) for both gallium samples Ga I and Ga II.

Reaction	Sample	γ energy (keV)	σ_{Ga}/σ_{Au}	u_{stat}	u_{syst}
^{69}Ga(n, γ)	Ga I	176	0.2820	0.0045	0.0198
		1039	0.3173	0.0045	0.0308
	Ga II	176	0.2692	0.0034	0.0189
		1039	0.3078	0.0033	0.0299
^{71}Ga(n, γ)	Ga I	601	0.1636	0.0055	0.0101
		630	0.1808	0.0024	0.0112
		834	0.1778	0.0017	0.0110
		894	0.1744	0.0041	0.0108
		1051	0.1731	0.0050	0.0107
	Ga II	601	0.1644	0.0051	0.0102
		630	0.1776	0.0019	0.0110
		834	0.1744	0.0011	0.0108
		894	0.1806	0.0035	0.0112
		1051	0.1611	0.0042	0.0099

C. Conclusion and outlook

In view of the so-far not understood discrepancies, we have decided to refrain from recommending new Maxwellian-averaged cross sections yet. We have performed further time-of-flight as well as activation measurements intended to solve the obviously puzzling situation. Further publications and a final evaluation of the MACSs will follow.

ACKNOWLEDGMENT

This project was supported by EFNUDAT, ERINDA, the EuroGENESIS project MASCHE, HIC for FAIR, BMBF (05P15RFFN1) and DFG (RE 3461/4-1).

[1] R. Reifarth, C. Lederer, and F. Käppeler, J. Phys. G **41**, 053101 (2014).
[2] F. Käppeler, R. Gallino, S. Bisterzo, and W. Aoki, Rev. Mod. Phys. **83**, 157 (2011).
[3] U. Frischknecht, R. Hirschi, M. Pignatari, A. Maeder, G. Meynet, C. Chiappini, F.-K. Thielemann, T. Rauscher, C. Georgy, and S. Ekström, Mon. Not. R. Astron. Soc. **456**, 1803 (2016).
[4] M. Pignatari, R. Gallino, M. Heil, M. Wiescher, F. Käppeler, F. Herwig, and S. Bisterzo, Astrophys. J. **710**, 1557 (2010).
[5] H. Nassar, M. Paul, I. Ahmad, D. Berkovits, M. Bettan, P. Collon, S. Dababneh, S. Ghelberg, J. P. Greene, A. Heger, M. Heil, D. J. Henderson, C. L. Jiang, F. Käppeler, H. Koivisto, S. O'Brien, R. C. Pardo, N. Patronis, T. Pennington, R. Plag, K. E. Rehm, R. Reifarth, R. Scott, S. Sinha, X. Tang, and R. Vondrasek, Phys. Rev. Lett. **94**, 092504 (2005).
[6] R. Reifarth, J. Phys.: Conf. Ser. **202**, 012022 (2010).
[7] V. N. Kononov, I. I. Stavisskii, and V. A. Tolstikov, Sov. J. At. Energ. **5**, 1483 (1958).
[8] N. Otuka, E. Dupont, V. Semkova, B. Pritychenko, A. Blokhin, M. Aikawa, S. Babykina, M. Bossant, G. Chen, S. Dunaeva,

R. Forrest, T. Fukahori, N. Furutachi, S. Ganesan, Z. Ge, O. Gritzay, M. Herman, S. Hlavač, K. Katc, B. Lalremruata, Y. Lee, A. Makinaga, K. Matsumoto, M. Mikhaylyukova, G. Pikulina, V. Pronyaev, A. Saxena, O. Schwerer, S. Simakov, N. Soppera, R. Suzuki, S. Takács, X. Tao, S. Taova, F. Tárkányi, V. Varlamov, J. Wang, S. Yang, V. Zerkin, and Y. Zhuang, Nucl. Data Sheets **120**, 272 (2014).

[9] A. K. Chaubey and M. L. Sehgal, Phys. Rev. **152**, 1055 (1966).

[10] R. L. Macklin, N. H. Lazar, and W. S. Lyon, Phys. Rev. **107**, 504 (1957).

[11] R. P. Anand, M. L. Jhingan, D. Bhattacharya, and E. Kondaiah, Nuovo Cimento A **50**, 247 (1979).

[12] G. Walter, H. Beer, F. Kaeppeler, G. Reffo, and F. Fabbri, Astron. Astrophys. **167**, 186 (1986).

[13] I. Dillmann, R. Plag, F. Käppeler, and T. Rauscher, *Proceedings of the Workshop EFNUDAT Fast Neutrons - Scientific Workshop on Neutron Measurements, Theory & Applications* (Geel, Belgium, 2009).

[14] A. G. Dovbenko, V. E. Kolesov, V. P. Koroleva, and V. A. Tolstikov, Sov. At. Energy **27**, 1185 (1969).

[15] G. Walter, KfK Bericht **3706** (1984).

[16] R. Reifarth, P. Erbacher, S. Fiebiger, K. Göbel, T. Heftrich, M. Heil, F. Käppeler, N. Klapper, D. Kurtulgil, C. Langer, C. Lederer-Woods, A. Mengoni, B. Thomas, S. Schmidt, M. Weigand, and M. Wiescher, Eur. Phys. J. Plus **133**, 424 (2018).

[17] K. Lodders, Lect. Notes Phys. **16**, 379 (2010).

[18] G. Gürdal and E. McCutchan, Nucl. Data Sheets **136**, 1 (2016).

[19] D. Abriola and A. Sonzogni, Nucl. Data Sheets **111**, 1 (2010).

[20] X. Huang and M. Kang, Nucl. Data Sheets **133**, 221 (2016).

[21] R. Reifarth, M. Heil, F. Käppeler, and R. Plag, Nucl. Instrum. Methods Phys. Res., Sect. A **608**, 139 (2009).

[22] W. Ratynski and F. Käppeler, Phys. Rev. C **37**, 595 (1988).

[23] G. Feinberg, M. Friedman, A. Krása, A. Shor, Y. Eisen, D. Berkovits, D. Cohen, G. Giorginis, T. Hirsh, M. Paul, A. J. M. Plompen, and E. Tsuk, Phys. Rev. C **85**, 055810 (2012).

[24] M. Chadwick, M. Herman, P. Obložinský, M. Dunn, Y. Danon, A. Kahler, D. Smith, B. Pritychenko, G. Arbanas, R. Arcilla, R. Brewer, D. Brown, R. Capote, A. Carlson, Y. Cho, H. Derrien, K. Guber, G. Hale, S. Hoblit, S. Holloway, T. Johnson, T. Kawano, B. Kiedrowski, H. Kim, S. Kunieda, N. Larson, L. Leal, J. Lestone, R. Little, E. McCutchan, R. MacFarlane, M. MacInnes, C. Mattoon, R. McKnight, S. Mughabghab, G. Nobre, G. Palmiotti, A. Palumbo, M. Pigni, V. Pronyaev, R. Sayer, A. Sonzogni, N. Summers, P. Talou, I. Thompson, A. Trkov, R. Vogt, S. van der Marck, A. Wallner, M. White, D. Wiarda, and P. Young, Nucl. Data Sheets **112**, 2887 (2011).

[25] B. Pritychenko and S. F. Mughabghab, Nucl. Data Sheets **113**, 3120 (2012).